

ARTICLE TYPE

# Calibrated river-level estimation from river-cameras using convolutional neural networks

Remy Vandaele<sup>1,4</sup><sup>\*</sup>, Sarah L. Dance<sup>1,2,3</sup> and Varun Ojha<sup>4</sup>

<sup>1</sup>Department of Meteorology, University of Reading, Reading, UK

<sup>2</sup>Department of Mathematics and Statistics, University of Reading, Reading, UK

<sup>3</sup>National Centre for Earth Observation, Reading, UK

<sup>4</sup>Department of Computer Science, University of Reading, Reading, UK

<sup>\*</sup>Corresponding author. E-mail: [r.a.vandaele@reading.ac.uk](mailto:r.a.vandaele@reading.ac.uk)

(Received DD Month YYYY; revised DD Month YYYY; accepted DD Month YYYY)

**Keywords:** River cameras, flooding, river levels, deep learning, convolutional neural networks

## Abstract

Monitoring river water-levels is essential for the study of floods and mitigating their risks. River gauges are a well-established method for river water-level monitoring but many flood-prone areas are ungauged and must be studied through gauges located several kilometers away. Taking advantage of river cameras to observe river water-levels is an accessible and flexible solution but it requires automation. However, current automated methods are only able to extract uncalibrated river water-level indexes from the images, meaning that these indexes are relative to the field of view of the camera, which limits their application. With this work, we propose a new approach to automatically estimate calibrated river water-level indexes from images of rivers. This approach is based on the creation of a new dataset of 32,715 images coming from 95 river cameras in the UK and Ireland, cross-referenced with gauge data (river water-level information) which allowed us to train convolutional neural networks. These networks are able to accurately produce two types of calibrated river water-level indexes from images: one for continuous river water-level monitoring, and one for flood event detection. This work is an important step towards the automated use of cameras for flood monitoring.

## Impact Statement

Floods are natural hazards that need to be monitored and studied in order to reduce their damage. This work explores a flexible solution to measure water-levels using a network of river cameras. River cameras are mounted in a fixed position, near a river, and stream images via the internet. The challenge with river cameras is to automate the extraction of the river water-levels, or a related index, from the images. The existing automated methods tackling this challenge are only able to produce water-level indexes that are not calibrated (relative to the camera field of view), which narrows their range of applications. This work is the first to propose a method that automatically estimates calibrated water-level indexes from images. For this purpose, a dataset of 95 cameras and 32,715 images cross-referenced with data from river water-level measurement gauge was created. This dataset was then used to train deep convolutional neural networks in order to produce a method able to extract calibrated river water-levels indexes from camera images. This work allows river cameras to be used for automated river water-level monitoring using calibrated indexes.

## 1. Introduction

Flood events are a recurring natural hazard causing injuries, homelessness, economic losses and deaths all over the world, every year (Guerreiro et al., 2018). The severity of floods is even increasing with climate change and growing human activity, such as building assets over land close to river banks (Alfieri et al., 2015). It is therefore necessary to employ effective and efficient techniques to monitor flood events to avoid economic, social, and human losses.

The forecasting and management of river flood events is complicated because of the difficulty of obtaining accurate measurements of river water-levels. Indeed, the river gauges commonly used to measure these levels can be overwhelmed during flood events. Another problem is that observing a flood by using gauges relies on scarce data making the studies difficult: gauge stations are typically constructed every 10-60km in Europe (Neal et al., 2009). Besides, their number is declining globally (Mishra and Coulibaly, 2009; Global Runoff Data Center, 2016).

There are also flood monitoring techniques based on satellite and aerial images either through expert observation and image processing (e.g., Mason et al. (2021); Mauro et al. (2021); Perks et al. (2016)) or through deep learning (e.g., Nemni et al. (2020)). When combined with a digital elevation model (DEM), they can be used to derive water-levels along the flood edge (see Grimaldi et al. (2016) for a review). These images can be obtained with optical sensors or synthetic aperture radar (SAR). However, satellite and airborne optical techniques are hampered by their daylight-only application and their inability to map flooding beneath clouds and vegetation (Yan et al., 2015). On the other hand, SAR images are unaffected by clouds and can be obtained day or night. Thus, their relevance for flood mapping in rural areas is well established (e.g., Mason et al. (2012); Alfieri et al. (2013); Giustarini et al. (2016)). In urban areas, shadow and layover issues make the flood mapping more challenging (e.g., Mason et al. (2018); Tanguy et al. (2017); Mason et al. (2021); Mauro et al. (2021)). In addition, SAR satellite overpasses are infrequent (at most once or twice per day, depending on location), so it is uncommon to capture the rising limb of the flood (Grimaldi et al., 2016), which prevents considering this technique for the live monitoring of floods.

Recently, new solutions have been considered in order to accurately monitor floods, and among them the use of river cameras has received significant attention (Tauro et al., 2018). River cameras are CCTV cameras, installed with a fixed field of view to observe a river. They provide a continuous stream of images and may be installed by individuals to monitor river water-levels for recreational purposes (fishing or boating for example) and are also used by public or private organisations for river monitoring purposes. They are flexible as they can rely on battery supplies and upload images through broadband/4G connections and can be easily installed (e.g., on trees, buildings or lamp posts). However, a limitation of this approach is the annotation of such images. Indeed, studies have considered studying floods through manually annotated camera images (e.g., Vetra-Carvalho et al. (2020)) but their manual annotation is complex, time consuming, and requires on-site ground-survey. In consequence, it is not possible to straightforwardly repeat this process manually on a large scale, and thus strongly limits the use of river cameras for flood monitoring.

There are existing initiatives that rely on crowd-sourcing approaches to share the burden of the annotation process (e.g. Etter et al., 2020; Lowry et al., 2019; Baruch, 2018). These processes are made accessible through the help of graphic tools such virtual gauges, and guidelines to help the annotator perform their annotation task and attribute a flood severity index to an image. However, it has been noted that the crowd-sourced annotations are often inaccurate and their number depends on the degree of investment of the volunteers involved with the project (Etter et al., 2020).

Several studies have already considered the development of deep learning and computer vision algorithms for flood monitoring via the semantic segmentation of water in images (the detection of pixels that contain water, e.g., Vandaele et al. (2021); Moy de Vitry et al. (2019)). However, on its own, the semantic segmentation of water is of limited interest when it comes to finding the (evolution of the)

water-level of the river in the image. Indeed, the first way to use the segmentation consists in taking a time series of images of the same camera to observe the relative evolution of the percentage of flooded pixels of (a region of) the image. However, it only allows production of an uncalibrated water-level index, dependent on the field of view of the camera (Moy de Vitry et al., 2019). The second solution is to carry out ground surveys in order to match the segmented water with the height of surveyed locations within the field of view to estimate the river water-level. However, carrying out ground surveys is impractical since spots of interest could be hard or even dangerous to access and field studies would drastically reduce the automation potential of river camera images. A third solution that would consist in merging the camera images with digital elevation models can only be performed manually at this stage, as current literature suggest that deep learning methods are not accurate enough to perform such tasks (Mertan et al., 2021). An object detection approach has also been considered to evaluate flood situations in urban areas (Rizk et al., 2022). However, this methodology relies on the deployment of drones and the presence of specific objects (flooded cars or houses), which limits the potential of the method to capture the rising limb of the flood (before the deployment of the drones and/or before the cars and homes get flooded). To the best of our knowledge, due to the lack of water-level specific datasets, there is no other deep learning approach considered for flood monitoring.

In this work we propose a new approach for extracting calibrated river water-level indexes from river camera images. This approach is able to produce two calibrated indexes: one for continuous river water-level monitoring, and one boolean for the detection of flood events. This approach is based on the creation of a large dataset of river camera images cross-referenced with river water-levels coming from nearby gauges to train deep learning networks. In consequence, we bring the following contributions:

- A dataset of images annotated with river water-levels, built by cross-referencing river cameras with nearby river water-level measurements produced by gauges.
- A deep learning methodology to train two deep convolutional neural networks (CNNs):
  - Regression-WaterNet, that is able to provide a continuous and calibrated river water-level index. This network is aimed at providing an index useful for the live monitoring of river water-levels.
  - Classification-WaterNet, that is able to discriminate river images observing flood situations from images observing unflooded situations. This network is aimed at providing local flood warnings that could enhance existing flood warning services.
- An analysis showing that our methodology can be used as a reliable solution to monitor flood events at ungauged locations.

We note that there are uncertainties in the dataset. Firstly, these are due to inaccuracies of gauge measurements (see McMillan et al. (2012) for a complete review). Secondly, uncertainties are introduced by the association of the camera with gauges that are not co-located (see Section 2.1). Nevertheless, our results demonstrate that river cameras and deep learning have a major potential for the critical task of river water-level monitoring in the context of flood events.

The rest of this manuscript is divided into three sections. Section 2 details the methodology used to develop the approach, including the building of the dataset, the definition of the calibrated indexes, and the development and training of the deep learning network that estimated calibrated river water-level indexes. Section 3 presents an analysis of the results obtained by the networks, notably through the comparison with water-level data from distant gauges. Finally, Section 4 presents our concluding remarks. More especially, our methodology is able to accurately produce two types of calibrated river water-level indexes from images: one for continuous river water-level monitoring, and one for flood event detection. This work is an important step towards the automated use of cameras for flood monitoring.

## 2. Methodology

The lack of a substantial dataset of flood images labelled with information relating to the severity of the flood situation is the foremost reason pointed out in Section 1 for the insufficient development of a deep learning model able to estimate a calibrated severity index of a flood situation from an image. This section describes the methodology that was employed for creating such a dataset and the process to develop and train the flood monitoring deep learning models called WaterNets on this dataset. Firstly, Section 2.1 explains the creation process for the large dataset of images where each image is labelled with a river water-level. Secondly, Section 2.2 details the different approaches considered to transform these river water-levels into calibrated indexes representing the severity of a flood situation. Finally, Section 2.3 presents the WaterNet CNN architectures that were used to learn the relationships between the images and their river water-levels from the dataset.

### 2.1. Creation of the dataset

This section discusses the preparation of the initial dataset that labels river camera images with river water-level measurements in metres. These measurements are either relative to a local stage datum (Above Stage Datum, mASD), or an ordnance datum (Above Ordnance Datum, mAOD, measured relative to the mean sea level). The transformation of these two types of river water-levels into calibrated indexes is presented in Section 2.2.

#### *Acquisition of the river water-levels.*

The various environmental agencies of the United Kingdom and the Republic of Ireland publicly provide data related to the river water-levels measured in the gauge stations distributed across their territories: Environment Agency (EA) in England (EA, 2021), Natural Resources Wales (NRW) in Wales (NRW, 2021), Scottish Environment Protection Agency (SEPA) in Scotland (SEPA, 2021), Department for Infrastructure (DfI) in Northern Ireland (DfI, 2021) and Office for Public Works (OPW) in the Republic of Ireland (OPW, 2021). In England, the EA only provides water-level data on an hourly basis for the last 12 months. Consequently, this work only considered the water-levels (and images) for the year 2020. For each gauge station, the EA also provides an API allowing the retrieval of the GPS coordinates of the gauges, as well as the name of the river on which they are located. The other agencies allow the retrieval of the GPS locations and rivers monitored through accessible graphical interfaces. In this paper, a gauge,  $g$ , produces pairs  $(w_g, t_g)$  where  $w_g$  is the water-level and  $t_g$  its timestamp. We suppose that there are  $L_g$  pairs, ordered by their timestamp. We refer to the  $i$ -th pair as  $(w_g(i), t_g(i))$ ,  $i \in [1, 2, \dots, L_g]$ .

#### *Acquisition of the images.*

We used the network of camera images maintained by Farson Digital Watercams<sup>1</sup> for the acquisition of the images. Farson Digital Watercams is a private company that installs cameras on waterways in the UK and the Republic of Ireland. The images from the cameras can be downloaded through an API (subject to an appropriate licensing agreement with the company). At the time of writing this paper, the company had 163 cameras operational. Among these cameras, 104 were installed in England, 9 in the Republic of Ireland, 5 in Northern Ireland, 38 in Scotland, and 7 in Wales. These cameras broadcast one image per hour, between 7 or 8 a.m. and 5 or 6 p.m. (local time). Apart from one camera that was removed from our considerations, the field of view of each camera includes a river, a lake, or the sea. At this stage, they were all kept in the dataset. The images from each camera are available since the installation of the camera, but there can be interruptions due to camera failure or maintenance. After inspection of the cameras, it was observed that a camera may be re-positioned occasionally depending on the wishes of a client, thus changing the field of view at that camera location. Five cameras were moved in 2020. The first cameras were installed in 2009, while the newest were installed in 2020. For

<sup>1</sup><https://www.farsondigitalwatercams.com>

each of these cameras, their GPS coordinates and the name of the river/lake/sea in its field of view can be retrieved through Farson Digital's API. In this paper, a camera,  $c$ , produces pairs  $(x_c, u_c)$  where  $x_c$  is the image and  $u_c$  its timestamp. We suppose that there are  $M_c$  pairs, ordered by their timestamp. We refer to the  $i$ -th pair as  $(x_c(i), u_c(i)), i \in [1, 2, \dots, M_c]$ .

#### Labelling camera images with river water-levels.

Each camera was first associated with the closest available gauge on the same river. This was done by computing the Euclidean distance between the gauges and the camera with the GPS coordinates (converted into GNSS) and by matching the river names. These attributes (camera and gauge GPS coordinates and river names) were retrieved using the EA and Farson Digital's APIs. If the river name was not available for the camera, the association was performed manually using the GPS coordinates and Google Maps. We defined a cut-off distance of 50km, and cameras that were located more than this distance away from the nearest gauge were removed. The cut-off distance was determined experimentally by making a trade-off between the number of camera images that we could use in the dataset and the proximity of the gauge to the camera. Note that due to a recent cyber-attack on the Scottish agency SEPA<sup>2</sup>, the gauge data monitored by SEPA was not available for this work, which forced us to remove most cameras located in Scotland.

Secondly, the remaining camera images were each labelled with the water-level measurement of the corresponding gauge by matching the timestamp of the image with a timestamp of a water-level recording. The water-level that was the closest-in-time to the image timestamp was chosen, if the measurement was made within a 30-minute time-range. If there was no such available water-level measurement, the camera image was discarded. This labelling process between a camera  $c$  and a gauge  $g$  is summarised in Algorithm 1.

---

#### Algorithm 1 Labelling camera $c$ images with water-level data from a gauge $g$

---

```

triplets is an empty set
 $i = 1$ 
while  $i \leq M_c$  do
     $j = 1$ 
     $w_{\text{best}} = -1$ 
     $\delta_{\text{best}} = \infty$ 
    while  $j \leq L_g$  do
         $\delta_{\text{current}} = |u_c(i) - t_g(j)|$ 
        if  $\delta_{\text{current}} < \delta_{\text{best}}$  then
             $w_{\text{best}} = w_g(j)$ 
             $\delta_{\text{best}} = \delta_{\text{current}}$ 
        end if
         $j = j + 1$ 
    end while
    if  $\delta_{\text{best}} < 30$  minutes then
        triplets = triplets  $\cup \{(x_c(i), u_c(i), w_{\text{best}})\}$ 
    end if
     $i = i + 1$ 
end while
return triplets




```

---




Finally, we performed a visual inspection of the remaining cameras in order to ensure that the situation described at the gauge station roughly matched the reality shown by the camera. This process is

<sup>2</sup><https://www.bbc.co.uk/news/uk-scotland-57578762> (last accessed 27 January 2022)

**A) Exebridge camera associated with EA gauge 45122**

Date	09:00, 07/06/2020	16:00, 18/08/2020	17:00, 16/02/2020
Gauge level	Low (0.07m)	Average (0.16m)	High (1.39m)
Image			
Association	<b>Good association</b>		

**B) Kintore camera associated with EA gauge L0001**

Date	09:00, 10/04/2020	08:00, 09/09/2020	13:00, 10/02/2020
Gauge level	Low (-1.75m)	Average (0.49m)	High (2.52m)
Image			
Association	<b>Bad association</b>		

**Figure 1.** Representation of the camera visual inspection process, as explained in Section 2.1. The first camera in Exebridge presented in A), associated with the EA gauge 45122 suggests a good association as the lowest, average, high water-levels are the labels of images where the water-levels are respectively low, average and high. The camera in Kintore presented in B), associated with the EA gauge L0001 suggests a bad association as the lowest, average and high water-levels are the water-level labels of camera images which are not in a similar situation.

depicted in Figure 1. During this visual inspection process, three images are extracted: a first labelled with one of the lowest water-level ( $< 5$ th percentile of the water-level heights used to label the camera images), a second labelled with an average water-level (within the 45 – 55th percentile interval), and a third labelled with one of the highest water-level ( $> 95$ th percentile). If the water-level visualised in the first image is lower than the one visualised in the second, and if the water-level visualised in the second image is lower than the one visualised in the third, the gauge association was successful (good association). If not, the gauge association has failed (bad association) and the camera is discarded from the dataset.

In this paper, the labelling process of the data  $(x_c, u_c)$  from a camera  $c$  generates triplets  $(x_c, u_c, w_c)$  where  $x_c$  is a camera image,  $u_c$  its timestamp and  $w_c$  its water-level label. We suppose that there are  $N_c$  triplets, with  $N_c \leq M_c$ , sorted according to their timestamp. We refer to the  $i$ -th triplet as  $(x_c(i), u_c(i), w_c(i)), i \in [1, 2, \dots, N_c]$ .

In most cases, the gauge data is not co-located with the camera. Even after the visual inspection, this introduces some uncertainties in the quantitative values of the indexes. Indeed, as they are not co-located, water-level values at the gauge may not perfectly match the situation at the camera location (due to differences in river bathymetry and local topography, arrival time of a flood-wave etc.). However, gauge data are the only suitable data that are routinely available without making additional



measurements in the field. Besides, for the experiments presented in Section 3, these uncertainties are minimised on our test cameras as the quality of the gauge association was inspected thoroughly.

### Size of the dataset.

Of the initial 163 cameras, 95 remained after the selection process. The number of images per camera is between 583 and 3,939 with a median number of 3,781 images per camera. The associated gauges are located within a radius of 7m to 42.1km, with 50% of these gauges within a radius of 1km to the camera. A total of 327,215 images of these cameras are labelled with river water-levels. Note that this large number of images comes from a limited number of 95 cameras, so there are about 100 different fields of views in the dataset (five cameras in the dataset were moved, so there are more than 95 fields of view).

## 2.2. Calibrated flood severity indexes

The previous Section 2.1 discussed the creation of a dataset of images labelled with water-levels. The water-levels labels are provided in metric units relative to either sea level (mAOD - Above Ordnance Datum) or a stage datum (mASD - Above Stage Datum) chosen according to the local configuration of their gauge station. Without additional topographic information on the site locations, these water-levels are thus not calibrated and do not allow observation of river water-levels from different cameras in a common reference system. However, a common reference system is necessary for training a model independent of site locations and camera fields of view.

This section outlines the two approaches that were considered in this work in order to calibrate the river water-level measurements obtained from the gauges to allow the observation of the river water-level from different cameras in a common reference system.

### 2.2.1. Standardized river water-level

The first approach that was considered was to transform the river water-levels  $w_g(i)$  into standardized river water-levels  $z_g(i)$  (z-scores) for each gauge  $g$  independently, subtracting the average water-level (for that gauge) from the water-level, and then dividing the residual by the standard deviation (for that gauge). This is summarised by the equation

$$z_g(i) = \frac{w_g(i) - \overline{w_g}}{\sqrt{\frac{1}{L_g} \sum_{j=1}^{L_g} (w_g(j) - \overline{w_g})^2}}, \quad (1)$$

where  $\overline{w_g} = \frac{1}{L_g} \sum_{k=1}^{L_g} w_g(k)$ .

With this approach, the gauge river water-levels of the cameras are in the same reference system. Indeed, the river water-levels of each gauge share a common mean 0 and variance 1. Also note that the reference (sea level or stage datum) has no impact on the definition of this index.

This index  $z_g(i)$  is thus a continuous metric for the monitoring of river water-levels. The higher the index is, the higher the water-level is.

These indexes are computed for each gauge, and then used to label the camera images following the association and labelling process explained in Section 2.1. In this case, this process generates triplets  $(x_c, u_c, z_c)$ . We refer to the  $i$ -th triplet as  $(x_c(i), u_c(i), z_c(i)), i \in [1, 2, \dots, N_c]$ .

### 2.2.2. Flood classification index

The second approach that was considered was to transform the river water-levels produced by a gauge  $g$  with a binary True/False index  $b_g(i)$ , where  $b_g(i)$  represents the flood situation (True if flooded, False otherwise), such that

$$b_g(i) = \begin{cases} \text{True}, & \text{if } w_g(i) > h_g, \\ \text{False}, & \text{otherwise} \end{cases}, \quad (2)$$

where  $h_g$  is a threshold specific to the gauge  $g$  producing the river water-level measurements.

According to the EA documentation (EA, 2021), the *Typical High* threshold of a gauge is set to the 95th-percentile of all the water-levels measured at that gauge since its installation. This threshold was chosen as the flood threshold  $h_g$  in this work. This threshold is available in the metadata for most EA gauges. When this threshold was not available as metadata (e.g., gauges in the Republic of Ireland), if a camera was associated with this gauge, it was removed for this specific experiment.

Similarly to the standardized river water-level, these indexes are computed for each gauge, and used to label the camera images following the association and labelling process explained in Section 2.1. In this case, this process generates triplets  $(x_c, u_c, b_c)$ . We refer to the  $i$ -th triplet as  $(x_c(i), u_c(i), b_c(i)), i \in [1, 2, \dots, N_c]$ .

### 2.3. WaterNet architectures and training

This work relies on a state-of-the-art ResNet-50 network that has among the best architectures for image classification tasks (He et al., 2016). We modified the last layer of this network in order to match our needs. Indeed, as we consider the estimation of two different river water-level indexes, we defined two corresponding network architectures for which the only difference is the last layer:

- For the Standardized river water-level index (see Section 2.2.1), the last layer of ResNet-50 was changed to a one neuron layer. We will refer to this network as **Regression-WaterNet**.
- For the Flood classification index (see Section 2.2.2), the last layer of ResNet-50 was changed to a two-neuron layer with the last layer being a SoftMax layer. We will refer to this network as **Classification-WaterNet**.

To train the networks, we chose to rely on a transfer learning approach which has already proven useful to improve the performance of water segmentation networks (Vandaele et al., 2021): before training the WaterNet networks over the labelled camera images, all the weights of the networks, except the last layer, were first set to the values obtained by training the network over the standard large dataset for image classification, ImageNet (Deng et al., 2009). They were then fine tuned over the labelled camera image dataset. With this transfer methodology, the initial setting of the convolutional layers weights is already efficient at processing image inputs as it was trained over a large multi purpose dataset of RGB images. Thus, it facilitates the training of the network for a new image processing task.

For both Regression-WaterNet and Classification-WaterNet, a grid search was performed to find the optimal learning parameters for training the networks (learning rate, percentage of network layers frozen to the values of the network trained over ImageNet (Deng et al., 2009), update factor, patience). The values tested are shown in Table 1. The networks were fine-tuned on the training set over 30 epochs. A L1 loss was used for Regression-WaterNet and a binary cross-entropy loss was used for Classification-WaterNet (Zhang et al., 2021). At each epoch, the network was evaluated on a validation set and the learning rate updated with an update factor if it was not improving for a number of epochs (patience). The weights of the WaterNet network trained with the learning parameters obtaining the best results on the validation set during the grid search were then used to evaluate the performance of the networks on the test set.

## 3. Experiments

This section describes the results of the experiments that were performed to assess the performance of the WaterNet networks. Two experiments were performed: the first, detailed in Section 3.1, was



Parameter	Values tested
Learning rate	$10^{-4}$ , $10^{-5}$ , $10^{-6}$
% layers frozen	0, 0.25, 0.5, 0.75, 0.9
Update factor	0.1, 0.5, 0.9
Patience	1,5,10,30

**Table 1.** Learning parameters tested during the grid search.

performed to assess the performance of Regression-WaterNet to estimate the standardized river water-level index. The second experiment, detailed in Section 3.2, assesses the performance of Classification-WaterNet for the estimation of the flood classification index.

### 3.1. Standardized river water-level index results using Regression-WaterNet

#### 3.1.1. Experimental design

##### *Dataset split.*

As presented in Section 2.1, the dataset at our disposal consisted of 95 cameras. This dataset was divided into three parts:

- The **test set** that consisted of the 15,107 images of 4 cameras that were chosen as these cameras have been previously studied by a human observer and their correspondence to nearby gauge-based water-level observations has been assessed (Vetra-Carvalho et al., 2020): Diglis Lock (abbreviated to Diglis), Evesham, Strensham Lock (abbreviated to Strensham) and Tewkesbury Marina (abbreviated to Tewkesbury). As shown in Figure 2, these 4 cameras offer 4 different site configurations. Their associated gauges were respectively located at 58m, 1.08km, 37m and 53m from the cameras.
- The **validation set** that consisted of the 18,894 images from 5 other cameras that were chosen randomly. We chose to rely on a relatively small sized validation set to keep a large number of different camera fields of view in the training set.
- The **training set** that consisted of the 293,214 images from the 86 remaining cameras and their images.

For this experiment, the images  $x_c$  are labelled with the standardized river water-level indexes  $z_c$  detailed in Section 2.2.1.

##### *Evaluation Protocol.*

In order to evaluate the efficiency of Regression-WaterNet, we report an error score that consists in the average of the absolute differences (also known as MAE - Mean Absolute Error) between the standardized water-level indexes  $z_c(i)$  of the image and the estimation of this standardized water-level index  $\hat{z}_c(i)$  over each of the  $N_c$  labelled images from the camera  $c$  using Regression-WaterNet such as

$$\text{MAE}_c = \frac{1}{N_c} \sum_{i=1}^{N_c} |z_c(i) - \hat{z}_c(i)| \quad (3)$$

Since to the best of our knowledge, we are the first to propose such a method, it is not possible to compare it to any other automated algorithm. However, it is possible to evaluate how well our methodology is working compared to using distant gauges in order to estimate the standardized river water-level at a given ungauged location. This evaluation is performed using the following protocol:

1. Each test camera is associated with:
  - A *reference gauge*, which is the gauge used to label its image water-levels, as described in Section 2.1. In the scope of our experiments, these gauges thus provide the *ground-truth* water-levels at the test camera locations.

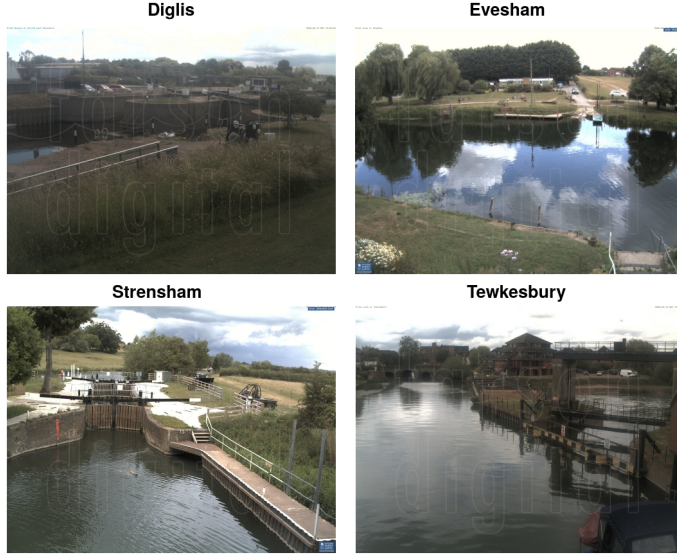


**Figure 2.** Sample images from the 4 cameras of the test set.

- The other gauges available within a 50km radius from its location. In the scope of our experiments, these are the *distant gauges*: they could be used to estimate the standardized river water-level index at the camera location if a reference gauge was not available.
2. We evaluate the accuracy of using a distant gauge to estimate the standardized river water-level at the camera location by comparing the standardized water-levels of the distant gauge with the standardized water-levels of the reference gauge.
    - The standardized water-levels of the distant and reference gauge are first matched according to their timestamp following a similar procedure than the image labelling procedure described in Algorithm 1.
    - The Mean Absolute Error (see Eq. 3) is computed between the associated standardized water-level indexes.
  3. The Mean Absolute Error obtained by each distant gauge can then be compared with the Mean Absolute Error obtained by our camera based methodology.

#### Processing the network outputs.

After its training following the protocol described in Section 2.3, Regression-WaterNet is able to estimate river water-level indexes from camera images. As the test cameras produce one image every hour (during daylight), the network generates a time-series of estimations that can potentially be post-processed. Two approaches were considered to post-process the time-series of estimations.

- **RWN**, where the time-series estimations of the Regression-WaterNet network  $\hat{z}_c(i)$  for each image  $x_c(i)$  are not post-processed and are thus considered independently. This is representative of cases where the goal would be to obtain independent measurements from single images.
- **Filtered RWN**, where the time series estimations of the Regression-WaterNet network  $\hat{z}_c(i)$  for each image  $x_c(i)$  are replaced by the median  $\hat{z}_c^F(i)$  of the estimations obtained from Regression-WaterNet on all the images available within a 10 hour time window such that

$$\hat{z}_c^F(i) = \text{median}(\{\hat{z}_c(j), |u_c(j) - u_c(i)| \leq 10 \text{ hours}\}), \quad (4)$$

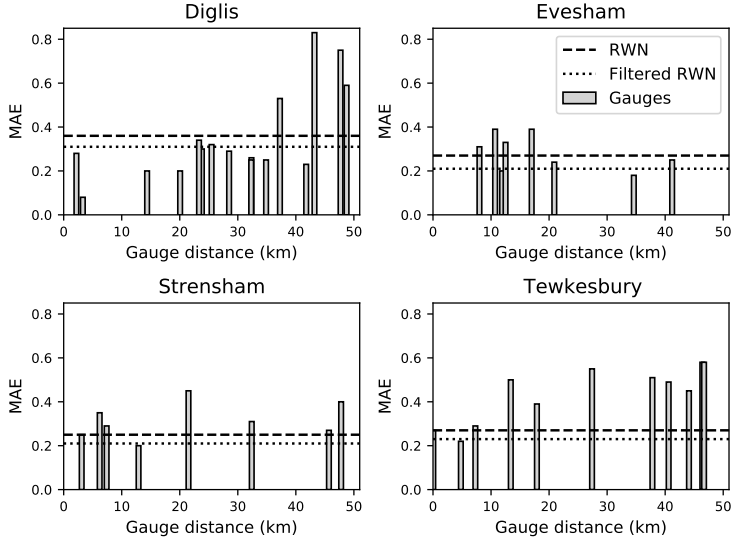


**Figure 3.** MAE scores obtained by applying RWN (dashed line) and Filtered-RWN (dotted line) on the camera images of Diglis, Evesham, Strensham and Tewkesbury. The bars represent the MAE scores obtained with the standardized river water-level indexes produced by the gauges within a 50km radius, as described in Section 3.1.1.

where, as explained in Section 2.1,  $u_c(i)$  corresponds to the timestamp of image  $x_c(i)$ . As the images are captured between 8am and 6pm, we chose this 10-hour time-window threshold so that the median would apply to all the images captured in the daylight hours of the same day.

### 3.1.2. Results and discussion

The comparison between the MAE obtained by the distant gauges and our methodology is given in Fig. 3. Overall, this figure shows that RWN and Filtered-RWN each allow the monitoring of the river water-level from the test cameras as accurately as a gauge within a 50km radius of the river camera. Indeed, compared to the gauges that were not associated with the camera, RWN offers among the best MAE for two locations (Evesham and Strensham) and average MAE for the two others (Diglis and Tewkesbury). The filtering process of Filtered-RWN decreases the error at each location. While there is always a gauge within 50km that is able to obtain results at least as accurate as RWN, the closest gauge (after the reference gauge) does not always provide the best performance (never, in this case).

In practice, given an ungauged location in need of river water-level monitoring, it is thus easier to rely on our camera based methodology than relying on the estimations made by a distant gauge. Indeed, using a distant gauge providing accurate measurements for the ungauged location would require validation data, which is impossible by definition. In consequence, applying RWN or Filtered-RWN on camera images is a most suitable choice.

Fig. 4 shows the time-series of the standardized index through the year estimated by RWN and Filtered RWN, compared with gauge data from the reference gauges of the test cameras. RWN brings a significant variability in the observations, but overall the networks are able to successfully observe the flood events (that occur in January, February, March and December) as well as the lower river level period between April and August. As expected, the median filter used with Filtered RWN reduces the variability of the image-derived observations, but also tends to underestimate the height of river water-levels, especially during high flow and flood events. Filtered RWN estimates an oscillation of the

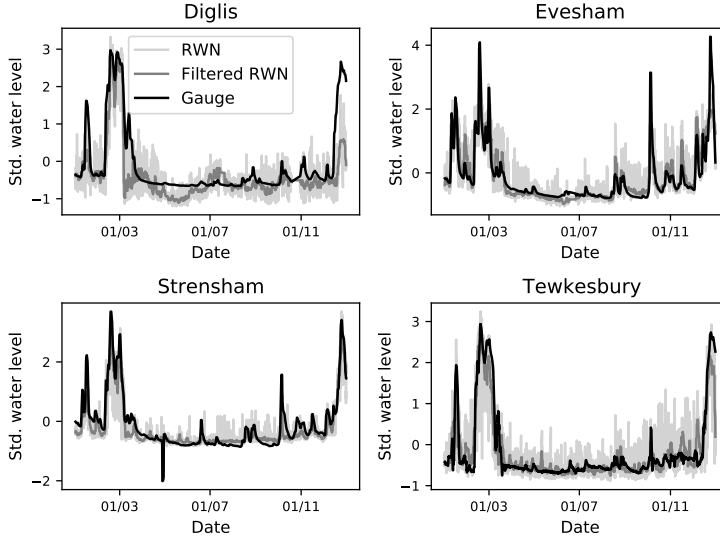


**Figure 4.** Monitoring of the river water-levels during 2020 at Diglis, Evesham, Strensham and Tewkesbury by applying RWN and Filtered-RWN to the camera images, compared to the river water-level data produced by the gauge associated with the camera.

standardized water-level at low water-levels at Diglis from March to July that is not explained by the gauge data nor by our visual inspection, and thus corresponds to estimation errors of the network.

After visual inspection, it was observed that the gauge measurements used to label camera images do not always perfectly match the situation at the camera location, so RWN sometimes gives a better representation of the situation than the standardized river water-levels of the gauges. For example, the gauge line in the Diglis plot in Fig. 4 suggests that the February and December floods in Diglis have reached the same level, while Filtered-RWN suggests that the December event was smaller than the March event. As suggested by Fig. 5, the largest flood extent observed in December at Diglis (24 December) does not reach the height of the largest flood extent observed in February (27 February). Another visible example is the significant sudden water-level drop at the Strensham gauge at the end of April, which is not visible in our image data. This is likely due to a gauge anomaly.

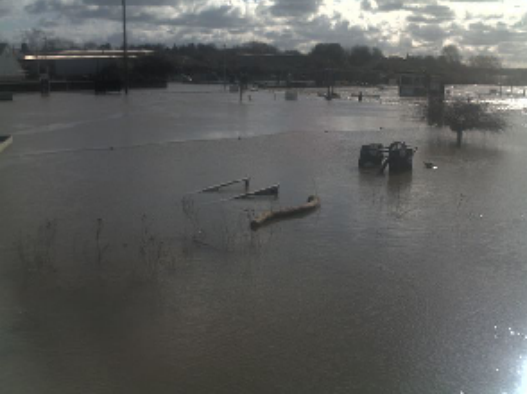
It can thus be concluded that the application of RWN and Filtered-RWN on river camera images allows to obtain results with similar accuracy to using water-level information from a gauge within a 50km radius.

### 3.2. Flood classification index results using Classification-WaterNet

#### 3.2.1. Experimental design

The experimental design used for this experiment is similar to the one used in the first experiment, described in Section 3.1.1. The same cameras were used for the training, validation and test splits. The images  $x_c$  were labelled with the binary flood indexes  $b_c$  detailed in Section 2.2.2. As explained in section 2.2.2, the water-level threshold that is considered for the separation between flooded and unflooded situations is defined as the 95th percentile of the water-level heights measured at the gauge since it was installed. This threshold value is obtained as metadata (the "typical high range" variable) alongside the water-level measurements from most EA gauges. Cameras for which we could not retrieve this threshold value were removed for this experiment (13 cameras belonging to the training set).

Flood 27/02 at Diglis



Flood 24/12 at Diglis



**Figure 5.** Camera images observing the flood event at Diglis, on 27 February 2020 (left), and on 24 December 2020 (right).

Given the definition of the typical high range threshold, there is a small number of images considered as flooded, which makes the training set imbalanced. The training of Classification-WaterNet was performed using an artificially augmented number of flooded images (through repetitions of the same flooded image, randomly flipped on their vertical axis) so that 50% of the images used in training were flooded situations.

Similarly to the protocol of the first experiment described in section 3.1.1, we post-processed the time-series estimations of Classification-WaterNet through two approaches:

- **CWN**, where the time-series estimations of the Classification-WaterNet network  $\hat{b}_c(i)$  for each image  $x_c(i)$  are not post-processed and thus considered independently. This is representative of cases where the goal would be to obtain independent measurements from single pictures.
- **Filtered CWN** outputs the estimated flood classification index  $\hat{b}_c^F(i)$ . In order to create this estimation, the output  $\hat{b}_c(i)$  of CWN is post-processed for each hour by replacing the independent estimation by the most represented class of estimations (flooded/not flooded) obtained within a 10 hour time window.

The following Balanced Accuracy criterion was used to evaluate the performance of the network:

$$\text{Balanced Accuracy} = 0.5 \times \frac{\text{TP}}{\text{TP} + \text{FP}} + 0.5 \times \frac{\text{TN}}{\text{TN} + \text{FN}}, \quad (5)$$

where

$$\begin{aligned} \text{TP} &= \#\{i | b_c(i) = \text{True}, \hat{b}_c(i) = \text{True}\}, \\ \text{FP} &= \#\{i | b_c(i) = \text{False}, \hat{b}_c(i) = \text{True}\}, \\ \text{TN} &= \#\{i | b_c(i) = \text{False}, \hat{b}_c(i) = \text{False}\}, \\ \text{FN} &= \#\{i | b_c(i) = \text{True}, \hat{b}_c(i) = \text{False}\}, \end{aligned} \quad (6)$$

where TP corresponds to the number (#) of correctly classified flooded images, (true positives), FP to the number of incorrectly classified unflooded images (false positives), TN to the number of correctly classified unflooded images (true negatives), and FN to the number of incorrectly classified flooded images (false negatives), such that

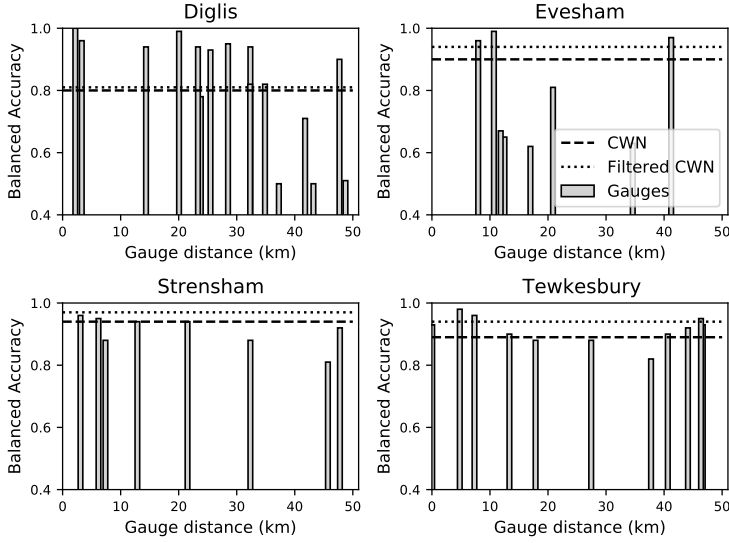


**Figure 6.** *Balanced Accuracy scores obtained by applying CWN (dashed line) and Filtered-CWN (dotted line) on the camera images of Diglis, Evesham, Strensham and Tewkesbury. The bars represent the Balanced Accuracy scores obtained by the gauges within a 50km radius producing a flood classification index, as described in Section 3.2.1.*

The Balanced Accuracy criterion gives a proportionate representation of the performance of Classification-WaterNet regarding the classification of flooded and unflooded images on the test set. Unlike the training set, the test set was not artificially augmented to contain a proportionate number of flooded and unflooded images.

Similarly to the first experiment (see Section 3.1.1), the performance of the network was also compared with an approach based on the flood classification indexes produced by nearby gauges (within a 50km radius), located on the same river. Given a reference gauge  $g_1$  and another gauge  $g_2$ ,

$$\begin{aligned}
 TP &= \#\{(i, j) | b_{g_1}(i) = \text{True}, \hat{b}_{g_2}(j) = \text{True}, t_{g_1} = t_{g_2}\}, \\
 FP &= \#\{(i, j) | b_{g_1}(i) = \text{False}, \hat{b}_{g_2}(j) = \text{True}, t_{g_1} = t_{g_2}\}, \\
 TN &= \#\{(i, j) | b_{g_1}(i) = \text{False}, \hat{b}_{g_2}(j) = \text{False}, t_{g_1} = t_{g_2}\}, \\
 FN &= \#\{(i, j) | b_{g_1}(i) = \text{True}, \hat{b}_{g_2}(j) = \text{False}, t_{g_1} = t_{g_2}\},
 \end{aligned} \tag{7}$$

where in this case  $g_1$  is the reference gauge attached to the camera. The Balanced Accuracy between the two gauges can then be computed with Eq. 5.

### 3.2.2. Results and discussion

Fig. 6 compares the Balanced Accuracy scores obtained by CWN and Filtered-CWN with the scores obtained by the nearby gauges producing the flood classification indexes. CWN obtains performance similar to the gauges with the highest Balanced Accuracy score at Evesham and Strensham, and Filtered-CWN at Tewkesbury. At Diglis, CWN and Filtered-CWN scores are average: they are significantly lower than the highest gauge-based Balanced Accuracy scores, but also significantly higher than the lowest ones.

By looking more closely at the results with the contingency table presented in Table 2, we can make two additional observations.



	TP	FP	TN	FN	Balanced Accuracy
Diglis	245 (+6)	15 (−8)	3239 (+8)	161 (−6)	0.8 (+0.01)
Evesham	118 (+8)	269 (−61)	3329 (+61)	16 (−8)	0.9 (+0.06)
Strensham	353 (+25)	43 (+9)	3383 (−9)	41 (−25)	0.94 (+0.03)
Tewkesbury	463 (+31)	524 (−240)	2873 (+240)	33 (−31)	0.89 (+0.07)

**Table 2.** Contingency table for the classification of flooded images using CWN. See Section 3.2.1 for the description of TP, FP, TN and FN. The changes brought with Filtered CWN are shown between the parentheses.

The first is that Filtered-CWN improves the Balanced Accuracy scores at each of the four locations. Filtered-CWN has a positive impact on the correction of both false positives and false negatives, except at Strensham where it slightly increased the number of false positives.

The second is that the network has a slight tendency to classify unflooded images as flooded at Evesham and Tewkesbury, and flooded images as not flooded at Diglis. However, from our visual analysis of the misclassified examples (see Fig. 7 for some examples), many of the images that the network falsely estimated as flooded in Evesham and Tewkesbury are images where the water-level is high and close to a flood situation, or seems to be actually flooded. The images wrongly estimated as not flooded at Diglis mostly represent situations where the river is still in bank. It thus seems that the network is prone to confusing borderline events where the river water-level is high but not necessarily high enough to produce a flood event. This can be explained by the fact that the high flow threshold used in this work to separate flooded images from unflooded ones is arbitrary and does not technically separate flooded images (when the river gets out-of-bank) from unflooded ones.

CWN and Filtered-CWN are able to obtain good performance at the four locations. (Filtered-)CWN has a slight tendency to confuse borderline cases of flood or non-flood events likely due to the arbitrary flood threshold used for the training and test cameras. However, when compared with distant gauge estimations using this arbitrary threshold, our results suggest that Classification-WaterNet could be used for flood detection.

## 4. Conclusions

The aim of this paper was to create deep learning based methods able to estimate calibrated river water-levels based on camera images in order to demonstrate the potential of river cameras combined with deep learning for the monitoring of rivers.

With the first part of this work, we have created a dataset of river camera images where each camera was associated to its closest river gauge measuring river water-levels. This dataset consists of 32,715 images coming from 95 different cameras across the UK and Ireland labelled with a river water-level value.

In the second part of this work, we used this dataset to train two deep convolutional neural networks. The first one, Regression-WaterNet, estimates standardized river water-level indexes from the images. The second one, Classification-WaterNet, detects flood situations from the images.

We were able to show that both networks were a reliable and convenient solution compared to using distant river gauges in order to perform the same river water-level monitoring tasks. Indeed, this solution provides river water-level index estimations as accurate as nearby gauges can provide. We also noticed that the performance of these methods might be better than the numerical evaluation of scores might indicate. Indeed, for both networks, we noticed after a visual inspection that some estimations considered by our numerical evaluation protocol were in fact more representative than the gauge measurements attached to the image.

The promising results of this study demonstrated the potential of deep learning methods on river cameras in order to monitor river water-levels, and more specifically floods. This represents a flexible, cost-effective and accurate alternative to more conventional means to monitor water-levels and floods in real-time and has potential to help in the prevention of further economic, social, and personal losses.

### Images falsely classified as flooded at Evesham



### Images falsely classified as flooded at Tewkesbury



### Images falsely classified as not flooded at Diglis



**Figure 7.** Examples of images misclassified by Classification-WaterNet.

**Acknowledgments.** The authors would like to thank Glyn Howells from Farson Digital Ltd for granting access to camera images. The authors would also like to thank David Mason, University of Reading, for the useful discussions.

**Funding Statement.** This research was supported in part by grants from the EPSRC(EP/P002331/1) and the NERC National Center for Earth Observation (NCEO).

**Competing Interests.** None

**Data Availability Statement.** The images used in this work are property of Farson Digital Watercams and can be downloaded on their website <https://www.farsondigitalwatercams.com/> subject to licensing conditions. The river gauge data can be found on the websites of the responsible authorities (EA, 2021; NRW, 2021; SEPA, 2021; DfI, 2021; OPW, 2021).

**Ethical Standards.** The research meets all ethical guidelines, including adherence to the legal requirements of the study country.

**Author Contributions.** Conceptualization: R.V. Methodology: R.V. Data curation: R.V. Data visualisation: R.V. Supervision: V.O;S.L.D. Funding acquisition: S.L.D. Writing original draft: R.V. Writing review and edition: V.O;S.L.D. Project Administration: S.L.D. All authors approved the final submitted draft.

## References

Alfieri, L., Burek, P., Dutra, E., Krzeminski, B., Muraro, D., Thielen, J., and Pappenberger, F. (2013). GloFAS—global ensemble streamflow forecasting and flood early warning. *Hydrology and Earth System Sciences*, 17(3):1161–1175.

- Alfieri, L., Burek, P., Feyen, L., and Forzieri, G. (2015). Global warming increases the frequency of river floods in Europe. *Hydrology and Earth System Sciences*, 19(5):2247–2260.
- Baruch, A. (2018). *An investigation into the role of crowdsourcing in generating information for flood risk management*. PhD thesis, Loughborough University.
- Deng, J., Dong, W., Socher, R., Li, L.-J., Li, K., and Fei-Fei, L. (2009). Imagenet: A large-scale hierarchical image database. In *2009 IEEE conference on computer vision and pattern recognition*, pages 248–255. Ieee.
- DfI (2021). DfI rivers water level network. <https://www.infrastructure-ni.gov.uk/articles/dfi-rivers-water-level-network>. [Online; accessed 30 November 2021].
- EA (2021). Environment Agency Real Time flood-monitoring API. <https://environment.data.gov.uk/flood-monitoring/doc/reference>. [Online; accessed 30 November 2021].
- Etter, S., Strobl, B., van Meerveld, I., and Seibert, J. (2020). Quality and timing of crowd-based water level class observations. *Hydrological Processes*, 34(22):4365–4378.
- Giustarini, L., Hostache, R., Kavetski, D., Chini, M., Corato, G., Schlaffer, S., and Matgen, P. (2016). Probabilistic flood mapping using synthetic aperture radar data. *IEEE Transactions on Geoscience and Remote Sensing*, 54(12):6958–6969.
- Global Runoff Data Center (2016). Global Runoff Data Base, temporal distribution of available discharge data. [https://www.bafg.de/SharedDocs/Bilder/Bilder\\_GRDC/grdcStations\\_tornadoChart.jpg](https://www.bafg.de/SharedDocs/Bilder/Bilder_GRDC/grdcStations_tornadoChart.jpg). Last visited:2021-04-26.
- Grimaldi, S., Li, Y., Pauwels, V. R., and Walker, J. P. (2016). Remote sensing-derived water extent and level to constrain hydraulic flood forecasting models: Opportunities and challenges. *Surveys in Geophysics*, 37(5):977–1034.
- Guerreiro, S. B., Dawson, R. J., Kilsby, C., Lewis, E., and Ford, A. (2018). Future heat-waves, droughts and floods in 571 European cities. *Environmental Research Letters*, 13(3):034009.
- He, K., Zhang, X., Ren, S., and Sun, J. (2016). Deep residual learning for image recognition. In *Proceedings of the IEEE conference on computer vision and pattern recognition*, pages 770–778.
- Lowry, C. S., Fienen, M. N., Hall, D. M., and Stepenuck, K. F. (2019). Growing Pains of Crowdsourced Stream Stage Monitoring Using Mobile Phones: The Development of CrowdHydrology. *Frontiers in Earth Science*, 7:128.
- Mason, D., Bevington, J., Dance, S., Revilla-Romero, B., Smith, R., Vetra-Carvalho, S., and Cloke, H. (2021). Improving urban flood mapping by merging synthetic aperture radar-derived flood footprints with flood hazard maps. *Water*, 13(1577).
- Mason, D., Schumann, G.-P., Neal, J., Garcia-Pintado, J., and Bates, P. (2012). Automatic near real-time selection of flood water levels from high resolution Synthetic Aperture Radar images for assimilation into hydraulic models: A case study. *Remote Sensing of Environment*, 124:705–716.
- Mason, D. C., Dance, S. L., Vetra-Carvalho, S., and Cloke, H. L. (2018). Robust algorithm for detecting floodwater in urban areas using synthetic aperture radar images. *Journal of Applied Remote Sensing*, 12(4):045011.
- Mauro, D., Hostache, R., Matgen, P., Pelich, R., Chini, M., van Leeuwen, P. J., Nichols, N. K., Blöschl, G., et al. (2021). Assimilation of probabilistic flood maps from sar data into a coupled hydrologic–hydraulic forecasting model: a proof of concept. *Hydrology and Earth System Sciences*, 25(7):4081–4097.
- McMillan, H., Krueger, T., and Freer, J. (2012). Benchmarking observational uncertainties for hydrology: rainfall, river discharge and water quality. *Hydrological Processes*, 26(26):4078–4111.
- Mertan, A., Duff, D. J., and Unal, G. (2021). Single image depth estimation: An overview. *arXiv preprint arXiv:2104.06456*.
- Mishra, A. K. and Coulibaly, P. (2009). Developments in hydrometric network design: A review. *Reviews of Geophysics*, 47(2).
- Moy de Vitry, M., Kramer, S., Wegner, J. D., and Leitão, J. P. (2019). Scalable flood level trend monitoring with surveillance cameras using a deep convolutional neural network. *Hydrology and Earth System Sciences*, 23(11):4621–4634.
- Neal, J., Schumann, G., Bates, P., Buytaert, W., Matgen, P., and Pappenberger, F. (2009). A data assimilation approach to discharge estimation from space. *Hydrological Processes: An International Journal*, 23(25):3641–3649.
- Nemni, E., Bullock, J., Belabbes, S., and Bromley, L. (2020). Fully convolutional neural network for rapid flood segmentation in synthetic aperture radar imagery. *Remote Sensing*, 12(16):2532.
- NRW (2021). River levels, rainfall and sea data. <https://rivers-and-seas.naturalresources.wales/>. [Online; accessed 30 November 2021].
- OPW (2021). Realtime waterlevel. <https://waterlevel.ie/>. [Online; accessed 30 November 2021].
- Perks, M. T., Russell, A. J., and Large, A. R. (2016). Advances in flash flood monitoring using unmanned aerial vehicles (UAVs). *Hydrology and Earth System Sciences*, 20(10).
- Rizk, H., Nishimur, Y., Yamaguchi, H., and Higashino, T. (2022). Drone-based water level detection in flood disasters. *International Journal of Environmental Research and Public Health*, 19(1):237.
- SEPA (2021). SEPA water level data. <https://www2.sepa.org.uk/waterlevels/>. [Online; accessed 30 November 2021].
- Tanguy, M., Chokmani, K., Bernier, M., Poulin, J., and Raymond, S. (2017). River flood mapping in urban areas combining Radarsat-2 data and flood return period data. *Remote Sensing of Environment*, 198:442–459.
- Tauro, F., Selker, J., Van De Giesen, N., Abrate, T., Uijlenhoet, R., Porfiri, M., Manfreda, S., Caylor, K., Moramarco, T., Benveniste, J., et al. (2018). Measurements and observations in the XXI century (MOXXI): innovation and multi-disciplinarity to sense the hydrological cycle. *Hydrological sciences journal*, 63(2):169–196.
- Vandaele, R., Dance, S. L., and Ojha, V. (2021). Deep learning for the estimation of water-levels using river cameras. *Hydrology and Earth System Sciences Discussions*, pages 1–29.
- Vetra-Carvalho, S., Dance, S. L., Mason, D. C., Waller, J. A., Cooper, E. S., Smith, P. J., and Tabcart, J. M. (2020). Collection and extraction of water level information from a digital river camera image dataset. *Data in Brief*, 33:106338.

- Yan, K., Di Baldassarre, G., Solomatine, D. P., and Schumann, G. J.-P. (2015). A review of low-cost space-borne data for flood modelling: topography, flood extent and water level. *Hydrological Processes*, 29(15):3368–3387.
- Zhang, A., Lipton, Z. C., Li, M., and Smola, A. J. (2021). Dive into deep learning. *arXiv preprint arXiv:2106.11342*.